

# Determination of Dark Energy by the Einstein Telescope: Comparing with CMB, BAO and SNIa Observations

W. Zhao,<sup>1</sup> C. Van Den Broeck,<sup>2</sup> D. Baskaran,<sup>1</sup> and T.G.F. Li<sup>2</sup>

<sup>1</sup>*School of Physics and Astronomy, Cardiff University, Cardiff, CF24 3AA, United Kingdom*

<sup>2</sup>*Nikhef – National Institute for Subatomic Physics,  
Science Park 105, 1098 XG Amsterdam, The Netherlands*

(Dated: May 6, 2019)

## Abstract

A design study is currently in progress for a third generation gravitational-wave (GW) detector called Einstein Telescope (ET). An important kind of source for ET will be the inspiral and merger of binary neutron stars (BNS) up to  $z \sim 2$ . If BNS mergers are the progenitors of short-hard  $\gamma$ -ray bursts, then some fraction of them will be seen both electromagnetically and through GW, so that the luminosity distance and the redshift of the source can be determined separately. An important property of these ‘standard sirens’ is that they are *self-calibrating*: the luminosity distance can be inferred directly from the GW signal, with no need for a cosmic distance ladder. Thus, standard sirens will provide a powerful independent check of the  $\Lambda$ CDM model. In previous work, estimates were made of how well ET would be able to measure a subset of the cosmological parameters (such as the dark energy parameter  $w_0$ ) it will have access to, assuming that the others had been determined to great accuracy by alternative means. Here we perform a more careful analysis by explicitly using the potential Planck CMB data as prior information for these other parameters. We find that ET will be able to constrain  $w_0$  and  $w_a$  with accuracies  $\Delta w_0 = 0.096$  and  $\Delta w_a = 0.296$ , respectively. These results are compared with projected accuracies for the JDEM Baryon Acoustic Oscillations (BAO) project and the SNAP Type Ia supernovae (SNIa) observations.

PACS numbers: 98.70.Vc, 98.80.Cq, 04.30.-w

## I. INTRODUCTION

In the past decade, various observations, including Type Ia supernovae (SNIa) [1], the temperature and polarization anisotropies power spectrum of the Cosmic Microwave Background (CMB) radiation [2], the baryon acoustic oscillations (BAO) peak in the distribution of SDSS luminous red galaxies [3], and weak gravitational lensing [4], have all suggested that the present Universe is undergoing an accelerated expansion. A possible explanation would be the presence of a fluid called dark energy, which should have positive density but negative pressure (for a review, see [5]). Understanding the physical character of dark energy, assuming it exists, is one of the main challenges of modern cosmology. A key question is then how well we will be able to differentiate between various dark energy models by measuring the dark energy equation of state (EOS) and its time evolution.

Currently, among the main methods to determine the dark energy EOS are observations of SNIa, CMB, and large scale structure. The capabilities of these methods will be improved significantly in the near future [6, 7]. However, we note that all these methods are based on the observations of various electromagnetic waves. In addition to these electromagnetic methods, the observation of gravitational waves (GW) will provide a new technique, where gravitational wave sources, in particular inspiraling and merging compact binaries, can be considered as standard candles, or *standard sirens* [8]. In the case of ground-based detectors, the idea is to use binaries composed of two neutron stars (BNS), or a neutron star and a black hole (NSBH). These are hypothesized to be at the origin of short-hard  $\gamma$ -ray bursts (shGRBs). In many cases it is possible to identify the host galaxy of a shGRB and determine its redshift. From the gravitational wave signal itself one would be able to measure the luminosity distance in an absolute way, without having to rely on a cosmic distance ladder: standard sirens are *self-calibrating*.

The use of GW standard sirens to measure the Hubble constant with a network of advanced ground-based detectors has been studied by Nissanke et al. [9], and with LISA (using extreme mass ratio inspirals) by MacLeod and Hogan [10]. Supermassive binary black holes may be useful to study dark energy with LISA [11–14]. Observations of BNS events with the Big Bang Observer (BBO) would also allow for dark energy studies [15].

Currently a third-generation ground based observatory called Einstein Telescope (ET) is undergoing a design study [16]. The latter would be able to see BNS inspirals up to redshifts of  $z \sim 2$  and NSBH events up to  $z \sim 8$ , corresponding to millions of sources over the course of several years, some fraction of which will have a detectable electromagnetic counterpart (e.g., a shGRB).

Sathyaprakash et al. have investigated how well cosmological parameters could be determined with ET assuming 1000 ‘useful’ sources [17]. Among the parameters which ET will have access to are

$$(H_0, \Omega_m, \Omega_k, w_0, w_a), \quad (1)$$

where  $H_0$  is the Hubble parameter at the current epoch,  $\Omega_m$  the density of matter by the critical density,  $\Omega_k$  a parameter related to spatial curvature, and  $w_0$  and  $w_a$  parameters determining the dark energy EOS and its time evolution (see below for more precise definitions). ET will not be able to arrive at a completely independent measurement of all these parameters at once. In [17] it was assumed that, e.g., all parameters except  $w_0$  had been measured by other means (electromagnetic or GW) and could be assumed known with arbitrary accuracy for all practical purposes. Here we continue this study in more depth, with a focus on the dark energy parameters  $w_0$  and  $w_a$ . Instead of assuming the other parameters to be exactly known, we will use the predicted CMB prior from Planck. CMB measurements give accurate values for  $H_0$ ,  $\Omega_m$ ,  $\Omega_k$ , but have large uncertainties in  $w_0$  and  $w_a$ . Heuristically, imposing this prior effectively ‘fixes’ the values of  $H_0$ ,  $\Omega_m$ ,  $\Omega_k$ . To measure  $w_0$ ,  $w_a$  with GW standard sirens is then an important check of the values obtained through electromagnetic means.

The outline of the paper is as follows. In Sec. II, we recall the basics of using short-hard  $\gamma$ -ray bursts as standard sirens in potential ET GW observations. We then discuss the determination of the dark energy parameters by the ET GW method alone, after which we impose the Planck CMB prior. In Sec. III, we discuss the capabilities of the JDEM BAO project and of the SNAP SNIa project, and a comparison as well as the potential combination with the ET GW method is given. In Sec. IV we conclude with a summary of our main results.

## II. SHORT-HAND $\gamma$ -RAY BURSTS AS A KIND OF STANDARD SIRENS

### A. The expanding universe and the dark energy

We will work with the Friedmann-Lemaître-Robertson-Walker (FLRW) universes, which are described by:

$$ds^2 = -dt^2 + a^2(t) \left\{ \frac{dr^2}{1 - kr^2} + r^2 d\theta^2 + r^2 \sin^2 \theta d\phi^2 \right\}, \quad (2)$$

where  $t$  is the cosmic time, and  $(r, \theta, \phi)$  are the comoving spatial coordinates. The parameter  $k = 0, 1, -1$  describes the flat, closed and open universe, respectively. The evolution of the scale

factor  $a(t)$  depends on the matter and energy contents of the universe. Within General Relativity, the equations governing this evolution are

$$\left(\frac{\dot{a}}{a}\right)^2 \equiv H^2 = \frac{8\pi G\rho_{tot}}{3} - \frac{k}{a^2}, \quad \frac{\ddot{a}}{a} = -\frac{4\pi G}{3}(\rho_{tot} + 3p_{tot}), \quad (3)$$

where  $\rho_{tot}$  and  $p_{tot}$  are the total energy density and pressure in the universe, and  $H$  is the Hubble parameter. Since in this paper we are mainly interested in the later stages of the evolution of the universe, where the radiation component can be ignored, we only take into account baryonic matter, dark matter, and dark energy. The baryon and dark matter are both modeled as pressureless dust. We will assume that the equation of state (EOS) of a dark energy component is responsible for the recent expansion of the Universe, which should be determined by observations. In this paper, we shall adopt a phenomenological form for the equation-of-state parameter  $w$  as a function of redshift  $z$ :

$$\begin{aligned} w(z) &\equiv p_{de}/\rho_{de} = w_0 + w_a(1-a) + \mathcal{O}[(1-a)^2] \\ &\simeq w_0 + w_a \frac{z}{1+z}. \end{aligned} \quad (4)$$

This form has been adopted by many authors, including the DETF (dark energy task force) group [6]. In the present epoch where  $z \simeq 0$ , we have  $w \simeq w_0$ .  $w_a$  describes the evolution of  $w$  to next-to-leading order in  $(1-a)$ . Since we are mostly interested in the later stages of the universe's evolution, higher order terms will be ignored.

The evolution of dark energy is determined by the energy conservation equation  $\dot{\rho}_{de} + 3H(\rho_{de} + p_{de}) = 0$ . By using the EOS of dark energy, Eq. (4), we find that

$$\rho_{de} = \rho_{de,0} \times E(z), \quad (5)$$

where  $\rho_{de,0}$  is the value of  $\rho_{de}$  at  $z = 0$ , and

$$E(z) \equiv (1+z)^{3(1+w_0+w_a)} e^{-3w_a z/(1+z)}. \quad (6)$$

Using Eq. (3), the Hubble parameter  $H$  then becomes

$$H(z) = H_0 \left[ \Omega_m(1+z)^3 + \Omega_k(1+z)^2 + (1 - \Omega_m - \Omega_k)E(z) \right]^{1/2}. \quad (7)$$

In this expression,  $\Omega_m \equiv 8\pi G\rho_{m,0}/3H_0^2$  is the density of matter (baryon as well as dark matter) relative to the critical density, and  $\Omega_k \equiv -k/H_0^2$  is the contribution of the spatial curvature.  $H_0$  is the Hubble parameter at the present epoch. Throughout this paper, we shall adopt a fiducial cosmological model with the following values for the parameters [2]:

$$w_0 = -1, \quad w_a = 0, \quad \Omega_b h_0^2 = 0.02267, \quad \Omega_c h_0^2 = 0.1131, \quad \Omega_k = 0, \quad h_0 = 0.705, \quad (8)$$

where  $h_0 = H_0/(100 \text{ km s}^{-1} \text{ Mpc}^{-1})$ . The other parameters are obtained as  $\Omega_m = \Omega_b + \Omega_c = 0.2736$ ,  $\Omega_{de} = 1 - \Omega_m - \Omega_k = 0.7264$ . In Sec. IID, the CMB prior for the dark energy determination will be discussed, where the perturbation parameters  $A_s$  and  $n_s$  (the amplitude and spectral index of primordial density perturbations, respectively) and the reionization parameter  $\tau$  (the optical depth of reionization) are also needed. In our fiducial model, we take these to be [2]

$$A_s = 2.445 \times 10^{-9}, \quad n_s = 0.96, \quad \tau = 0.084. \quad (9)$$

To conclude this subsection, we state the expression for the luminosity distance  $d_L$  of the astrophysical sources as a function of redshift  $z$  (see, e.g., [6]):

$$d_L(z) = (1+z) \begin{cases} |k|^{-1/2} \sin \left[ |k|^{1/2} \int_0^z \frac{dz'}{H(z')} \right] & (\Omega_k < 0), \\ \int_0^z \frac{dz'}{H(z')} & (\Omega_k = 0), \\ |k|^{-1/2} \sinh \left[ |k|^{1/2} \int_0^z \frac{dz'}{H(z')} \right] & (\Omega_k > 0), \end{cases} \quad (10)$$

where  $|k|^{1/2} \equiv H_0 \sqrt{|\Omega_k|}$ . This formula will be used frequently in the subsequent discussion.

## B. Short-hard $\gamma$ -ray bursts and gravitational waves

Current observational studies of dark energy strongly rely on *standard candles*, i.e., sources for which the intrinsic luminosity is assumed to be known within a certain tolerance so that they can be used to determine luminosity distance. A widely used standard candle is the Type Ia supernova (SNIa) [1, 18]. The intrinsic luminosity of distant SNIa needs to be calibrated by comparison with different kinds of closer-by sources, leading to a ‘cosmic distance ladder’. This is not the case with GW standard sirens. As pointed out by Schutz, the chirping GW signals from inspiraling compact binary stars (neutron stars and black holes) can provide an absolute measure of distance, with no dependence on other sources [8]. The GW amplitude depends on the so-called chirp mass (a certain combination of the component masses) and the luminosity distance. However, the chirp mass can already be measured from the signal’s phasing, so that the luminosity distance can be extracted from the amplitude.

Before discussing standard sirens in more detail, let us first recall some basic facts about the gravitational radiation emitted by inspiraling compact binaries. Gravitational waves are described by a second rank tensor  $h_{\alpha\beta}$ , which, in the so-called transverse-traceless gauge, has only two independent components  $h_+$  and  $h_\times$ ,  $h_{xx} = -h_{yy} = h_+$ ,  $h_{xy} = h_{yx} = h_\times$ , all other components being zero. A detector measures only a certain linear combination of the two components, called

the response  $h(t)$ , which is given by (see, e.g., [19])

$$h(t) = F_+(\theta, \phi, \psi)h_+(t) + F_\times(\theta, \phi, \psi)h_\times(t), \quad (11)$$

where  $F_+$  and  $F_\times$  are the detector antenna pattern functions,  $\psi$  is the polarization angle, and  $(\theta, \phi)$  are angles describing the location of the source on the sky, relative to the detector. In general these angles are time-dependent, but for ground-based detectors the kind of signal we are interested in will tend to be in the sensitivity band for a sufficiently short duration that  $(\theta, \phi, \psi)$  can be considered constant[32].

Consider a coalescing binary at a luminosity distance  $d_L$ , with component masses  $m_1$  and  $m_2$ . Write  $M = m_1 + m_2$  for the total mass and  $\eta = m_1 m_2 / M^2$  for the symmetric mass ratio, and define the ‘chirp mass’ as  $\mathcal{M}_c = M\eta^{3/5}$ . Then to leading order in amplitude, the GW polarizations are

$$h_+(t) = 2\mathcal{M}_c^{5/3}d_L^{-1}(1 + \cos^2(\iota))\omega^{2/3}(t_0 - t) \cos[2\Phi(t_0 - t; M, \eta) + \Phi_0], \quad (12)$$

$$h_\times(t) = 4\mathcal{M}_c^{5/3}d_L^{-1}\cos(\iota)\omega^{2/3}(t - t_0) \sin[2\Phi(t_0 - t; M, \eta) + \Phi_0], \quad (13)$$

where  $\iota$  is the angle of inclination of the binary’s orbital angular momentum with the line-of-sight,  $\omega(t_0 - t)$  the angular velocity of the equivalent one-body system around the binary’s centre-of-mass, and  $\Phi(t_0 - t; M, \eta)$  the corresponding orbital phase. The parameters  $t_0$  and  $\Phi_0$  are constants giving the epoch of merger and the orbital phase of the binary at that epoch, respectively.

During the inspiral, the change in orbital frequency over a single period is negligible, and it is possible to apply a stationary phase approximation to compute the Fourier transform  $\mathcal{H}(f)$  of the time domain waveform  $h(t)$ . One has

$$\mathcal{H}(f) = \mathcal{A}f^{-7/6} \exp \left[ i(2\pi f t_0 - \pi/4 + 2\psi(f/2) - \varphi_{(2,0)}) \right], \quad (14)$$

where the Fourier amplitude  $\mathcal{A}$  is given by

$$\mathcal{A} = \frac{1}{d_L} \sqrt{F_+^2(1 + \cos^2(\iota))^2 + F_\times^2 4 \cos^2(\iota)} \sqrt{\frac{5\pi}{96}} \pi^{-7/6} \mathcal{M}_c^{5/6}. \quad (15)$$

The functions  $\psi$  and  $\varphi_{(2,0)}$  are

$$\psi(f) = -\psi_0 + \frac{3}{256\eta} \sum_{i=0}^7 \psi_i (2\pi M f)^{i/3}, \quad (16)$$

$$\varphi_{(2,0)} = \tan^{-1} \left( -\frac{2 \cos(\iota) F_\times}{(1 + \cos^2(\iota)) F_+} \right). \quad (17)$$

The parameters  $\psi_i$  can be found in [19].  $\mathcal{H}(f)$  is taken to be zero outside a certain frequency range. The upper cutoff frequency is dictated by the last stable orbit (LSO), which marks the end

of the inspiral regime and the onset of the final merger. We will assume that this occurs when the radiation frequency reaches  $f_{\text{upper}} = 2f_{\text{LSO}}$ , with  $f_{\text{LSO}} = 1/(6^{3/2}2\pi M)$  the orbital frequency at LSO.

In this paper we shall focus on the observation of GW sources by the Einstein Telescope (ET), a third generation ground-based gravitational wave detector. Although the basic design of ET is still under discussion, one possibility is to have three interferometers with  $60^\circ$  opening angles and 10km arm lengths, arranged in an equilateral triangle [16]. The corresponding antenna pattern functions are:

$$\begin{aligned} F_+^{(1)}(\theta, \phi, \psi) &= \frac{\sqrt{3}}{2} \left[ \frac{1}{2}(1 + \cos^2(\theta)) \cos(2\phi) \cos(2\psi) - \cos(\theta) \sin(2\phi) \sin(2\psi) \right], \\ F_\times^{(1)}(\theta, \phi, \psi) &= \frac{\sqrt{3}}{2} \left[ \frac{1}{2}(1 + \cos^2(\theta)) \cos(2\phi) \sin(2\psi) + \cos(\theta) \sin(2\phi) \cos(2\psi) \right], \\ F_{+,\times}^{(2)}(\theta, \phi, \psi) &= F_{+,\times}^{(1)}(\theta, \phi + 2\pi/3, \psi), \\ F_{+,\times}^{(3)}(\theta, \phi, \psi) &= F_{+,\times}^{(1)}(\theta, \phi + 4\pi/3, \psi). \end{aligned} \quad (18)$$

The performance of a GW detector is characterized by the one-side noise *power spectral density*  $S_h(f)$  (PSD), which plays an important role in the signal analysis. We take the noise PSD of ET to be [20][33]

$$S_h(f) = S_0 \left[ x^{p_1} + a_1 x^{p_2} + a_2 \frac{1 + b_1 x + b_2 x^2 + b_3 x^3 + b_4 x^4 + b_5 x^5 + b_6 x^6}{1 + c_1 x + c_2 x^2 + c_3 x^3 + c_4 x^4} \right], \quad (19)$$

where  $x \equiv f/f_0$  with  $f_0 = 200\text{Hz}$ , and  $S_0 = 1.449 \times 10^{-52} \text{Hz}^{-1}$ . The other parameters are as follows:

$$\begin{aligned} p_1 &= -4.05, & p_2 &= -0.69, \\ a_1 &= 185.62, & a_2 &= 232.56, \\ b_1 &= 31.18, b_2 = -64.72, b_3 = 52.24, & b_4 &= -42.16, b_5 = 10.17, b_6 = 11.53 \\ c_1 &= 13.58, c_2 = -36.46, & c_3 &= 18.56, c_4 = 27.43. \end{aligned} \quad (20)$$

For data analysis proposes, the noise PDS is assumed to be essentially infinite below a certain lower cutoff frequency  $f_{\text{lower}}$  (see the review [19]). For ET we take this to be  $f_{\text{lower}} = 1 \text{ Hz}$ .

The waveforms in Eq. (14) depend on the seven free parameters  $(\ln \mathcal{M}_c, \ln \eta, t_0, \psi_0, \cos(\iota), \psi, \ln d_L)$ ; note that for ‘useful’ events the sky position will be known. In order to deal with the parameter estimation, we employ the Fisher matrix approach [21]. In the case of a single interferometer  $A$  ( $A = 1, 2, 3$ ), the Fisher matrix is given by

$$\Lambda_{ij}^{(A)} = \langle \mathcal{H}_i^{(A)}, \mathcal{H}_j^{(A)} \rangle, \quad \mathcal{H}_i^{(A)} = \partial \mathcal{H}^{(A)}(f) / \partial p_i, \quad (21)$$

where  $\mathcal{H}^{(A)}$  is the output of interferometer  $A$ , and the  $p_i$  denote the free parameters to be estimated. The angular brackets denote the scalar product, which, for any two functions  $a(t)$  and  $b(t)$  is defined as

$$\langle a, b \rangle = 4 \int_{f_{\text{lower}}}^{f_{\text{upper}}} \frac{\tilde{a}(f)\tilde{b}^*(f) + \tilde{a}^*(f)\tilde{b}(f)}{2} \frac{df}{S_h(f)}, \quad (22)$$

where  $\tilde{a}$  and  $\tilde{b}$  are the Fourier transforms of the functions  $a(t)$  and  $b(t)$ . The Fisher matrix for the combination of the three interferometers is then

$$\Lambda_{ij} = \sum_{A=1}^3 \Lambda_{ij}^{(A)}. \quad (23)$$

The inner product also allows us to write the signal-to-noise ratios  $\rho^{(A)}$ ,  $A = 1, 2, 3$  in a compact way:

$$\rho^{(A)} = \sqrt{\langle \mathcal{H}^{(A)}, \mathcal{H}^{(A)} \rangle}. \quad (24)$$

The combined signal-to-noise ratio for the network of the three interferometers is then

$$\rho = \left[ \sum_{A=1}^3 \left( \rho^{(A)} \right)^2 \right]^{1/2}. \quad (25)$$

In this paper, we shall focus on the estimation of the parameter  $\ln d_L$ . The  $1\text{-}\sigma$  observational error,  $\sigma_o$ , can be estimated from the Fisher matrix  $\Lambda_{ij}$ . An important point is that shGRBs are believed to be beamed: the  $\gamma$  radiation is emitted in a narrow cone more or less perpendicular to the plane of the inspiral. We will assume that the total beaming angle is at most  $40^\circ$  [22] (corresponding to  $\iota \leq 20^\circ$ ), and a distinction will be made between two cases:

- The case of ‘strong beaming’: the beaming can be assumed to be so tight that one can take  $\iota = \psi = 0$ , and these parameters are not taken into account in the Fisher analysis. The  $1\text{-}\sigma$  errors are averaged over sky position.
- The ‘realistic’ case:  $\cos(\iota)$  and  $\psi$  are taken into account as parameters to be estimated. The  $1\text{-}\sigma$  errors from the Fisher matrix are averaged over both sky position  $(\theta, \phi)$  and orientation  $(\iota, \psi)$ , but with the constraint that  $\iota \leq 20^\circ$ .

We will assume that shGRBs are produced by the mergers of the neutron star binaries. For definiteness we take them to have component masses of  $(1.4, 1.4)M_{\text{sun}}$ . We will assume 1000 sources up to a redshift of  $z = 2$ , which is where the angle-averaged signal-to-noise ratio approximately reaches the value 8 in both the strong beaming and the realistic case. Angle-averaged errors in  $d_L$



are very nearly linear in  $z$ , and we will approximate them as such, taking the values at  $z = 1$  as a reference. (This actually means that at  $z = 2$ , we over-estimate the distance errors by almost 20%, so we are making a conservative choice.) In particular, we take

$$\sigma_0 = 0.065 z \quad (\text{strong beaming case}) \quad (26)$$

$$\sigma_0 = 0.12 z \quad (\text{realistic case}) \quad (27)$$

In practice, the measured distance also suffers from errors due to the effects of weak lensing. As in previous work [17] we assume the contribution to the distance error from weak lensing to satisfy  $\sigma_l = 0.05z$  in both the strong beaming and realistic cases. Thus, the total uncertainty on  $\Delta \ln d_L$  is taken to be

$$\Delta \ln d_L = \sqrt{\sigma_o^2 + \sigma_l^2}. \quad (28)$$

### C. Gravitational wave standard sirens

Now let us turn to the determination of the cosmological parameters, including dark energy parameters, by the GW standard sirens. For each shGRB source, the luminosity distance  $d_L$  is measured from the GW observation, and the redshift  $z$  can be obtained from the electromagnetic counterpart. Thus, the  $d_L - z$  relation can be employed to constrain various cosmological parameters. For the cosmological model introduced in Sec. II A, we consider five free parameters  $(w_0, w_a, \Omega_m, \Omega_k, h_0)$  which can be constrained by GW standard sirens. We note that the value of  $\Omega_{de}$  (the relative energy density of the dark energy component) is determined by the quantities  $\Omega_m$  and  $\Omega_k$  through  $\Omega_{de} \equiv 1 - \Omega_m - \Omega_k$ .

In order to estimate the errors on these parameters, we study a Fisher matrix  $F_{ij}^{\text{GW}}$  for a collection of inspiral events:

$$F_{ij}^{\text{GW}} = \sum_k \frac{\partial_i(\ln d_L(z_k)) \partial_j(\ln d_L(z_k))}{(\Delta \ln d_L(z_k))^2}, \quad (29)$$

where the index  $k = 1, 2, \dots$ , labels the events. The indices  $i$  and  $j$  run from 1 to 5, denoting the free parameters  $(w_0, w_a, \Omega_m, \Omega_k, h_0)$ , respectively. Eq. (10) gives the expression for  $d_L$ , the partial derivatives with respect to the parameters are evaluated at the parameter values corresponding to the fiducial cosmological model of Sec. II A, and  $\Delta \ln d_L$  is calculated using (28).

If the number of the sources is large, sum over events in (29) can be replaced by an integral,

$$F_{ij}^{\text{GW}} = \int_0^2 \frac{\partial_i(\ln d_L) \partial_j(\ln d_L)}{(\Delta \ln d_L)^2} f(z) dz, \quad (30)$$

where  $f(z)$  is the number distribution of the GW sources over redshift  $z$ . The upper integration limit  $z = 2$  is the redshift at which the angle-averaged signal-to-noise ratio in both the strong beaming and realistic cases is approximately 8. The number distribution  $f(z)$  is given by

$$f(z) = \frac{4\pi\mathcal{N}r(z)d_C^2(z)}{H(z)(1+z)}, \quad (31)$$

where  $d_C$  is the comoving distance, which is defined as  $d_C(z) \equiv \int_0^z 1/H(z')dz'$ . The function  $r(z)$  describes the time evolution of the burst rate, and the constant  $\mathcal{N}$  (the number of the sources per co-moving volume at redshift  $z = 0$  over the observation period) is fixed by requiring the total number of the sources  $N_{\text{GW}} = \int_0^2 f(z)dz$ . The expected total number of inspirals per year within the horizon of ET is  $\sim \text{several} \times 10^5$  for neutron star binaries. If, as suspected, neutron star binaries are the progenitors of the shGRBs [22], it might be possible to make a coincident detection of a significant subset of the events in the GW and electromagnetic windows, which can then be considered as standard sirens. As we have mentioned, shGRBs are believed to be beamed with small beaming angle, so only a small fraction of the total neutron star binaries are expected to be observed as shGRBs. Following [17], we assume that about 1000 events ( $\sim 10^{-3}$  of the total binary coalescences) will be observed in both windows, i.e.,  $N_{\text{GW}} = 1000$  throughout this paper.

Since the time evolution of the source rate is as yet unclear, in this paper we shall consider two different forms for the function  $r(z)$ . In the first case we assume that the sources are distributed uniformly, i.e., with constant comoving number density throughout the redshift range  $0 \leq z \leq 2$  (hereafter we will refer to this as the uniform distribution). In this case we have  $r(z) = 1$ , which is what was assumed in the previous work [17]. In the other case, we take  $r(z)$  to be the following function:  $r(z) = (1 + 2z)$  for  $z \leq 1$ ,  $r(z) = (15 - 3z)/4$  for  $1 < z < 5$ , and  $r(z) = 0$  for  $z \geq 5$ . This distribution is suggested by [23]. Hereafter, we shall call this the non-uniform distribution. In Fig. 1, we plot the distribution function  $f$  as a function of redshift  $z$  in the two cases. Note that in the case with non-uniform distribution, the sources are a little more concentrated at  $z = 1$ . In what follows we will find out how this affects the uncertainties on the cosmological parameters.

Using the definition (30), we can calculate the the Fisher matrix  $F_{ij}^{\text{GW}}$  for the following four combinations: *a. the strong beaming case with uniform distribution; b. the realistic case with uniform distribution; c. the strong beaming case with non-uniform distribution; d. the realistic case with non-uniform distribution.* The results are listed in Table I, II, III, IV.

From the Fisher matrices, we can calculate the  $1\text{-}\sigma$  uncertainties on the parameters, which are  $\Delta p_i = \sqrt{(F^{\text{GW}})^{-1}_{ii}}$ . For the strong beaming case with uniform distribution, by using the results

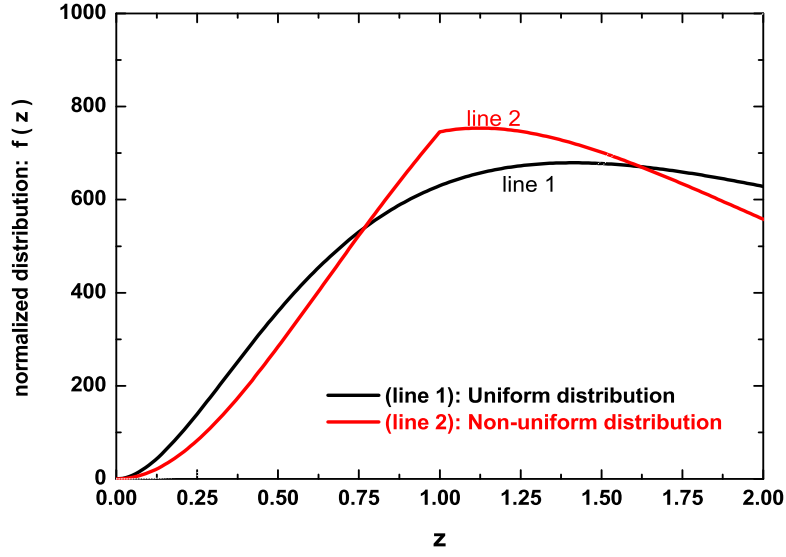


FIG. 1: The normalized distribution of the GW sources.

TABLE I: GW Fisher matrix in the strong beaming case and for the uniform distribution

|            | $w_0$                  | $w_a$                  | $\Omega_m$             | $\Omega_k$             | $h_0$                  |
|------------|------------------------|------------------------|------------------------|------------------------|------------------------|
| $w_0$      | $0.680235 \times 10^4$ | $0.103916 \times 10^4$ | $0.181422 \times 10^5$ | $0.654985 \times 10^4$ | $0.568452 \times 10^5$ |
| $w_a$      | $0.103916 \times 10^4$ | $0.175544 \times 10^3$ | $0.299868 \times 10^4$ | $0.983792 \times 10^3$ | $0.774727 \times 10^4$ |
| $\Omega_m$ | $0.181422 \times 10^5$ | $0.299868 \times 10^4$ | $0.516903 \times 10^5$ | $0.171593 \times 10^5$ | $0.141202 \times 10^6$ |
| $\Omega_k$ | $0.654985 \times 10^4$ | $0.983792 \times 10^3$ | $0.171593 \times 10^5$ | $0.635380 \times 10^4$ | $0.549739 \times 10^5$ |
| $h_0$      | $0.568452 \times 10^5$ | $0.774727 \times 10^4$ | $0.141202 \times 10^6$ | $0.549739 \times 10^5$ | $0.582070 \times 10^6$ |

TABLE II: GW Fisher matrix in the realistic case and for the uniform distribution

|            | $w_0$                  | $w_a$                  | $\Omega_m$             | $\Omega_k$             | $h_0$                  |
|------------|------------------------|------------------------|------------------------|------------------------|------------------------|
| $w_0$      | $0.270685 \times 10^4$ | $0.413513 \times 10^3$ | $0.721934 \times 10^4$ | $0.260637 \times 10^4$ | $0.226203 \times 10^5$ |
| $w_a$      | $0.413513 \times 10^3$ | $0.698542 \times 10^2$ | $0.119326 \times 10^4$ | $0.391479 \times 10^3$ | $0.308286 \times 10^4$ |
| $\Omega_m$ | $0.721934 \times 10^4$ | $0.119326 \times 10^4$ | $0.209690 \times 10^5$ | $0.682819 \times 10^4$ | $0.561884 \times 10^5$ |
| $\Omega_k$ | $0.260637 \times 10^4$ | $0.391479 \times 10^3$ | $0.682819 \times 10^4$ | $0.252836 \times 10^4$ | $0.218757 \times 10^5$ |
| $h_0$      | $0.226203 \times 10^5$ | $0.308286 \times 10^4$ | $0.561884 \times 10^5$ | $0.218757 \times 10^5$ | $0.231622 \times 10^6$ |

TABLE III: GW Fisher matrix in the strong beaming case and for the non-uniform distribution

|            | $w_0$                  | $w_a$                  | $\Omega_m$             | $\Omega_k$             | $h_0$                  |
|------------|------------------------|------------------------|------------------------|------------------------|------------------------|
| $w_0$      | $0.627650 \times 10^4$ | $0.101463 \times 10^4$ | $0.173966 \times 10^5$ | $0.602542 \times 10^4$ | $0.486282 \times 10^5$ |
| $w_a$      | $0.101463 \times 10^4$ | $0.176731 \times 10^3$ | $0.299310 \times 10^4$ | $0.958619 \times 10^3$ | $0.730442 \times 10^4$ |
| $\Omega_m$ | $0.173966 \times 10^5$ | $0.299310 \times 10^4$ | $0.509778 \times 10^5$ | $0.164126 \times 10^5$ | $0.128237 \times 10^6$ |
| $\Omega_k$ | $0.602542 \times 10^4$ | $0.958619 \times 10^3$ | $0.164126 \times 10^5$ | $0.582914 \times 10^4$ | $0.469111 \times 10^5$ |
| $h_0$      | $0.486282 \times 10^5$ | $0.730442 \times 10^4$ | $0.128237 \times 10^6$ | $0.469111 \times 10^5$ | $0.421176 \times 10^6$ |

TABLE IV: GW Fisher matrix in the realistic case and for the non-uniform distribution

|            | $w_0$                  | $w_a$                  | $\Omega_m$             | $\Omega_k$             | $h_0$                  |
|------------|------------------------|------------------------|------------------------|------------------------|------------------------|
| $w_0$      | $0.249760 \times 10^4$ | $0.403750 \times 10^3$ | $0.692263 \times 10^4$ | $0.239769 \times 10^4$ | $0.193505 \times 10^5$ |
| $w_a$      | $0.403750 \times 10^3$ | $0.703267 \times 10^2$ | $0.119104 \times 10^4$ | $0.381462 \times 10^3$ | $0.290664 \times 10^4$ |
| $\Omega_m$ | $0.692263 \times 10^4$ | $0.119104 \times 10^4$ | $0.202855 \times 10^5$ | $0.653105 \times 10^4$ | $0.510296 \times 10^5$ |
| $\Omega_k$ | $0.239769 \times 10^4$ | $0.381462 \times 10^3$ | $0.653105 \times 10^4$ | $0.231958 \times 10^4$ | $0.186672 \times 10^5$ |
| $h_0$      | $0.193505 \times 10^5$ | $0.290664 \times 10^4$ | $0.510296 \times 10^5$ | $0.186672 \times 10^5$ | $0.167598 \times 10^6$ |

in Table I, we find that

$$\Delta w_0 = 1.69, \Delta w_a = 5.95, \Delta \Omega_m = 0.514, \Delta \Omega_k = 1.30, \Delta h_0 = 7.00 \times 10^{-3}. \quad (32)$$

We plot the 2-dimensional uncertainty contour of the parameters  $w_0$  and  $w_a$  in Fig. 2 (blue curve, i.e. line 2, in the left panel). Unfortunately, we find that the error bars on the parameters are all fairly large, especially for the dark energy parameters  $w_0$  and  $w_a$ . This is caused by the strong degeneracy between  $(w_0, w_a)$  and the other parameters  $(\Omega_m, \Omega_k, h_0)$ , especially  $(\Omega_m, \Omega_k)$ . To illustrate this, let us do the following calculation. First we fix the values of the parameters  $(\Omega_m, \Omega_k, h_0)$  to be their fiducial values, and only consider  $(w_0, w_a)$  as free parameters. By using the results in Table I, we obtain

$$\Delta w_0 = 0.039, \Delta w_a = 0.244. \quad (33)$$

We find that the values of  $\Delta w_0$  and  $\Delta w_a$  become much smaller in this case. The 2-dimensional uncertainty contour of  $w_0$  and  $w_a$  is also plotted in Fig. 2 (black curve, i.e. line 1, in the left panel). This figure shows that there is correlation between the parameters  $w_0$  and  $w_a$ . Recall that a goal of the dark energy programs is to test whether dark energy arises from a simple cosmological constant,

( $w_0 = -1$ ,  $w_a = 0$ ). For a given data set we can do better (as far as excluding the cosmological constant model is concerned) than simply quoting the values of  $\Delta w_0$  and  $\Delta w_a$ . This is because the effect of dark energy is generally not best constrained at  $z = 0$ . For the phenomenological form of the EOS of the dark energy  $w(z) = w_0 + w_a z / (1 + z)$ , the constraint on  $w(z)$  varies with the redshift  $z$ . So, similar to [6], we can define the best pivot redshift, denoted as  $z_p$ , where the uncertainty in  $w(z)$  equals the uncertainty in a model that assumes  $w_a = 0$ . In this paper, we denote the EOS at this best pivot redshift as  $w_p \equiv w(z_p)$ . The best pivot redshift  $z_p$  can be calculated by  $z_p = -1 / (1 + \frac{\Delta w_a}{\rho \Delta w_0})$ , where  $\rho$  is the correlation coefficient of  $w_0$  and  $w_a$ . The value of  $\Delta w_p$  is calculated by  $\Delta w_p = \Delta w_0 \sqrt{1 - \rho^2}$ . In this case (two free parameters), the results for  $z_p$  and  $\Delta w_p$  are

$$z_p = 0.180, \quad \Delta w_p = 0.012. \quad (34)$$

The value of  $\Delta w_p$  as well as that of  $\Delta w_a$  are commonly used to describe the detection ability of the experiments [6].

On the other hand, we can also fix the values of the parameters ( $w_0$ ,  $w_a$ ) to be their fiducial values, and only consider ( $\Omega_m$ ,  $\Omega_k$ ,  $h_0$ ) as free parameters. By using the results in Table I, we obtain

$$\Delta \Omega_m = 0.014, \quad \Delta \Omega_k = 0.056, \quad \Delta h_0 = 3.22 \times 10^{-3}. \quad (35)$$

Again we find that the values of these errors, especially the values of  $\Delta \Omega_m$  and  $\Delta \Omega_k$ , are much smaller than those in Eq. (32). These results show that the GW standard sirens can constrain the dark energy parameters rather well, on condition that we can break the strong degeneracy between the parameters ( $w_0$ ,  $w_a$ ) and the parameters ( $\Omega_m$ ,  $\Omega_k$ ,  $h_0$ ). In the next subsection, we will find that this can be realized if we consider the CMB observations as a prior.

To conclude this subsection we discuss the determination of the dark energy parameters ( $w_0$ ,  $w_a$ ) by ET observations in all four cases considered in this paper. By using the results in Table I, II, III, IV, we calculate the errors of the two parameters (the other parameters are fixed at their fiducial values). The 2-dimensional uncertainty contours are shown in Fig. 3 (upper left panel). This figure shows that the errors of the parameters are a little larger in the realistic cases in the corresponding strong beaming cases. This is as expected, since the value of  $\Delta \ln d_L$  is larger in the realistic case than that in the strong beaming case. By comparing the black and red lines in this figure, we also find that the errors of the parameters are a little larger for the non-uniform distribution than those in the corresponding case with the uniform distribution. This is because

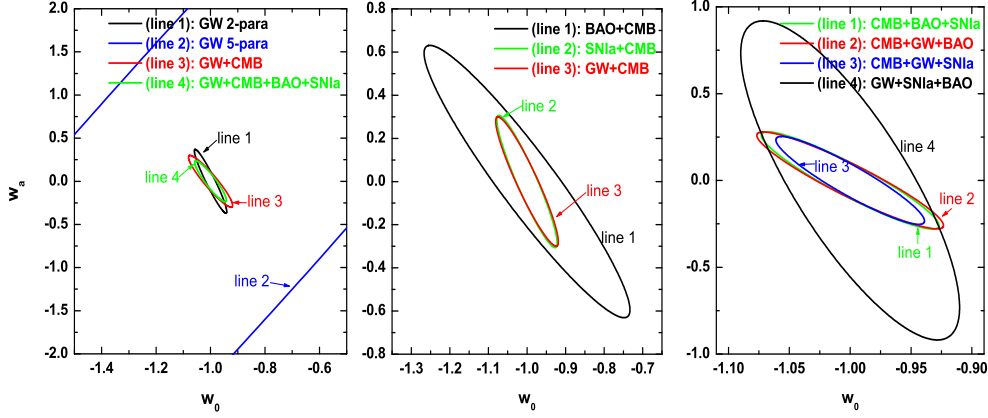


FIG. 2: The 2-d uncertainty contours of the dark energy parameters  $w_0$  and  $w_a$  in the strong beaming case and with uniform distribution.

the sources in the non-uniform distribution are a little more concentrated at the redshift  $z = 1$ . Hence the number of the sources in the high redshift and the low redshift regions is smaller, making it more difficult to constrain the dark energy's evolution. So, in addition to the number of the sources, the redshift distribution of the sources also plays a crucial role for the detection of dark energy. The results listed in (33) constitute the most optimistic case among the four cases we have considered. On the other hand, it is helpful to list the results in the most pessimistic case (realistic case and non-uniform distribution), which are

$$\Delta w_0 = 0.075, \quad \Delta w_a = 0.445. \quad (36)$$

We find that these uncertainties are nearly two times larger than those in (33). We can also calculate the values of  $z_p$  and  $\Delta w_p$  for this case, which are

$$z_p = 0.193, \quad \Delta w_p = 0.020. \quad (37)$$

The value of  $\Delta w_p$  is 67% larger than that in the optimistic case (strong beaming case with uniform distribution).

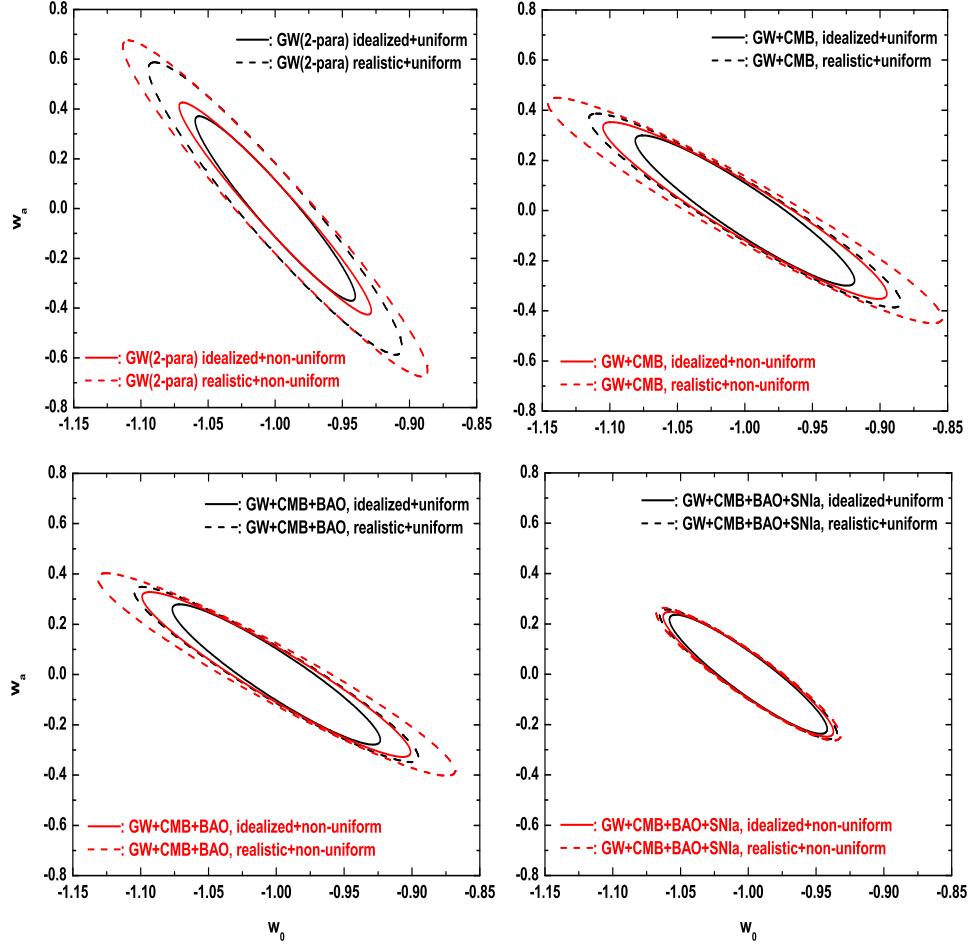


FIG. 3: The 2-d uncertainty contours for the dark energy parameters  $w_0$  and  $w_a$ , in the different cases.

#### D. Planck CMB prior

As will be clear from the discussion above, the ability of GW sources to constrain dark energy depends strongly on how well the background parameters  $\Omega_m$  and  $\Omega_k$  can be measured beforehand. Indeed, if one tries to determine these background parameters as well as the dark energy parameters together using GW sources, the values of  $\Delta w_0$  and  $\Delta w_a$  become very large, and the constraints on dark energy become meaningless. Hence we should consider another observational method which

can determine these background parameters as a prior observation. As we shall see, this is also necessary for the other ways used to study dark energy – BAO and SNIa – so that it does not diminish the value of having self-calibrating standard sirens: GW observations will provide us with an important independent check.

Observations of the Cosmic Microwave Background (CMB) temperature and polarization anisotropies are always used as the required prior. The WMAP satellite has already given fairly good results for the CMB  $TT$  (temperature-temperature auto-correlation) and  $TE$  (temperature-polarization cross correlation) power spectra in the multipole range  $\ell < 800$ . The background parameters ( $\Omega_m, \Omega_k$ ) have already been well determined by 7-year WMAP observations; for example, the constraint on the curvature is  $-0.0133 < \Omega_k < 0.0084$  (95%C.L.) [2]. These constraints are expected to be greatly improved by the Planck observations [24], which will give good data on the CMB  $TT$  and  $TE$  power spectra up to  $\ell \sim 2000$ . In addition, Planck is also expected to observe the  $EE$  (electric type polarization) power spectrum. In this subsection, we shall consider the potential CMB observations by the Planck satellite. For the noise power spectra of Planck, we consider the instrumental noises at three frequency channels: at 100GHz, 143GHz, and 217GHz. For the reduced foreground radiations (including dust and synchrotron), we assume that the reduced factor  $\sigma^{\text{fg}} = 0.1$ , i.e. 10% residual foregrounds are considered as the noises. The total noise power spectra  $N_\ell^{TT}$  and  $N_\ell^{EE}$  of the Planck satellite can be found in [25]. Note that in this paper we assume 4 sky (28 months) survey.

In order to estimate the constraints on the cosmological parameters, we shall again use the Fisher information matrix technique. The Fisher matrix is calculated by [26]

$$F_{ij}^{\text{CMB}} = \sum_{\ell=2}^{\ell_{\text{max}}} \sum_{XX', YY'} \frac{\partial C_\ell^{XX'}}{\partial p_i} \text{Cov}^{-1}(D_\ell^{XX'}, D_\ell^{YY'}) \frac{\partial C_\ell^{YY'}}{\partial p_j}, \quad (38)$$

where  $p_i$  are the cosmological parameters to be evaluated.  $C_\ell^{XX'}$  are the CMB power spectra and  $D_\ell^{XX'}$  are their estimates.  $\text{Cov}^{-1}$  is the inverse of the covariance matrix. The non-vanishing



components of the covariance matrix are given by

$$\begin{aligned}
\text{Cov}(D_\ell^{XX}, D_\ell^{XX}) &= \frac{2}{(2\ell+1)f_{\text{sky}}} (C_\ell^{XX} + N_\ell^{XX})^2 \quad (X = T, E), \\
\text{Cov}(D_\ell^{TE}, D_\ell^{TE}) &= \frac{1}{(2\ell+1)f_{\text{sky}}} [(C_\ell^{TE})^2 + (C_\ell^{TT} + N_\ell^{TT})(C_\ell^{EE} + N_\ell^{EE})], \\
\text{Cov}(D_\ell^{TT}, D_\ell^{EE}) &= \frac{2}{(2\ell+1)f_{\text{sky}}} (C_\ell^{TE})^2, \\
\text{Cov}(D_\ell^{TT}, D_\ell^{TE}) &= \frac{2}{(2\ell+1)f_{\text{sky}}} C_\ell^{TE} (C_\ell^{TT} + N_\ell^{TT}), \\
\text{Cov}(D_\ell^{EE}, D_\ell^{TE}) &= \frac{2}{(2\ell+1)f_{\text{sky}}} C_\ell^{TE} (C_\ell^{EE} + N_\ell^{EE}).
\end{aligned}$$

Note that in the calculation we have adopted  $\ell_{\text{max}} = 2000$ , and the sky-cut factor  $f_{\text{sky}} = 0.65$  suggested by Planck Bluebook [24].

The CMB power spectra  $C_\ell^{XX'}$  depend on all the cosmological parameters, including the background parameters and the perturbation parameters. In the calculation, we first build the Fisher matrix for the full nine parameters  $(w_0, w_a, \Omega_b h_0^2, \Omega_c h_0^2, \Omega_k, n_s, A_s, h_0, \tau)$ . In order to obtain the constraint on the parameter  $\Omega_m$ , we change the full Fisher matrix to the new one of the nine parameters  $(w_0, w_a, \Omega_m, \Omega_c h_0^2, \Omega_k, n_s, A_s, h_0, \tau)$ , where  $\Omega_m = (\Omega_b h_0^2 + \Omega_c h_0^2)/h_0^2$  has been used. In order to directly compare and combine with the Fisher matrix of GW method, we marginalize the new nine parameters Fisher matrix to the five parameters  $(w_0, w_a, \Omega_m, \Omega_k, h_0)$ . The results are shown in Table V. The errors of the parameters are given by  $\Delta p_i = \sqrt{(F^{\text{CMB}})^{-1}_{ii}}$ . By using the Fisher matrix in table V, we obtain

$$\Delta w_0 = 0.411, \quad \Delta w_a = 0.517, \quad \Delta \Omega_m = 8.88 \times 10^{-2}, \quad \Delta \Omega_k = 2.27 \times 10^{-3}, \quad \Delta h_0 = 0.115. \quad (39)$$

This result shows that Planck alone can give quite tight constraints on  $\Omega_m$  and  $\Omega_k$ , which is just complementary with the GW method. However, CMB observations alone cannot constrain the parameters  $w_0$  and  $w_a$ , which is because that the CMB power spectra are only sensitive to the physics in the early Universe at  $z \sim 1100$ , where dark energy is totally subdominant.

We now investigate the combination of CMB and GW methods. In order to do this, we define a new Fisher matrix, which is the sum of  $F_{ij}^{\text{GW}}$  and  $F_{ij}^{\text{CMB}}$ . By using this new Fisher matrix, we obtain

$$\Delta w_0 = 0.053, \quad \Delta w_a = 0.197, \quad \Delta \Omega_m = 3.69 \times 10^{-3}, \quad \Delta \Omega_k = 6.47 \times 10^{-4}, \quad \Delta h_0 = 3.67 \times 10^{-3}, \quad (40)$$

for the optimistic case (strong beaming and uniform distribution of GW sources). We find that the values of  $\Delta w_0$  and  $\Delta w_a$  are fairly close to those in Eq. (33), where we have only considered the

TABLE V: CMB Fisher matrix

|            | $w_0$                   | $w_a$                   | $\Omega_m$              | $\Omega_k$              | $h_0$                   |
|------------|-------------------------|-------------------------|-------------------------|-------------------------|-------------------------|
| $w_0$      | $0.414303 \times 10^5$  | $0.115085 \times 10^5$  | $0.287229 \times 10^6$  | $-0.678690 \times 10^6$ | $0.339923 \times 10^6$  |
| $w_a$      | $0.115085 \times 10^5$  | $0.320204 \times 10^4$  | $0.797415 \times 10^5$  | $-0.190373 \times 10^6$ | $0.943498 \times 10^5$  |
| $\Omega_m$ | $0.287229 \times 10^6$  | $0.797415 \times 10^5$  | $0.219854 \times 10^7$  | $-0.465663 \times 10^7$ | $0.251813 \times 10^7$  |
| $\Omega_k$ | $-0.678690 \times 10^6$ | $-0.190373 \times 10^6$ | $-0.465663 \times 10^7$ | $0.136912 \times 10^8$  | $-0.548091 \times 10^7$ |
| $h_0$      | $0.339923 \times 10^6$  | $0.943498 \times 10^5$  | $0.251813 \times 10^7$  | $-0.548091 \times 10^7$ | $0.291587 \times 10^7$  |

GW observations but assumed the background parameters  $\Omega_m$ ,  $\Omega_k$  and  $h_0$  are fixed. These results shows that taking the CMB observation as a prior is nearly equivalent to fixing the parameters  $\Omega_m$ ,  $\Omega_k$  and  $h_0$ . The 2-dimensional uncertainty contour of the parameters  $w_0$  and  $w_a$  is shown in Fig. 2 (red lines, i.e. line 3, in the left panel and the middle panel). We can also calculate the best pivot redshift  $z_p$  and the value of  $\Delta z_p$ , which are

$$z_p = 0.337, \quad \Delta w_p = 0.020. \quad (41)$$

By the same method, we also obtain the results in the other three cases. The 2-dimensional uncertainty contour of  $w_0$  and  $w_a$  is shown in Fig. 3 (upper-right panel). In the pessimistic case (realistic case and non-uniform distribution), the results are

$$\Delta w_0 = 0.096, \quad \Delta w_a = 0.296, \quad \Delta \Omega_m = 6.90 \times 10^{-3}, \quad \Delta \Omega_k = 6.70 \times 10^{-4}, \quad \Delta h_0 = 8.44 \times 10^{-3}. \quad (42)$$

The best pivot redshift  $z_p$  and the uncertainty  $\Delta w_p$  are

$$z_p = 0.447, \quad \Delta w_p = 0.029. \quad (43)$$

Again as expected, we find that the values are larger than the corresponding values in the optimistic case.

### III. DETECTION OF DARK ENERGY BY BAO AND SNIA OBSERVATIONS, AND THE COMPARISON WITH ET GW OBSERVATIONS

In the above we found that by combining the potential Planck CMB observation with ET GW observations, one can get fairly tight constraints on the dark energy parameters  $w_0$  and  $w_a$ . In this section we discuss the detection abilities of the other two probes: BAO and SNIa. Currently these two methods play the crucial role for the determination of the dark energy component. In the near

future, the detection abilities of these two methods are expected to be significantly improved; in this section a detailed discussion is given. All three probes, BAO, SNIa and GW, constrain the EOS of dark energy by probing the large-scale background geometry of the universe (different from the weak gravitational lensing method [27]), so a fair comparison can be made, as we shall do here.

### A. Detection of dark energy by potential BAO observations

The BAO method relies on the distribution of baryonic matter to infer the redshift-distance relation. The characteristic scale length of structure which can be accurately determined from the CMB is used as a standard rod. By measuring the angular size of this characteristic scale-length as a function of redshift, the effect of dark energy can be inferred. The BAO method can constrain the dark energy by two observable quantities  $\ln(H(z))$  and  $\ln(d_A(z))$ , where  $H(z)$  is the binned Hubble parameter and  $d_A(z)$  is comoving angular diameter distance, which is related to the luminosity distance by  $d_A = d_L/(1+z)$ . Similar to the quantity  $d_L$ , these two observables only depend on the cosmological parameters  $w_0$ ,  $w_a$ ,  $\Omega_m$ ,  $\Omega_k$  and  $h_0$ , which will be considered as the parameters determined by the observations.

In order to investigate the constraints on the cosmological parameters, we build the following Fisher information matrix [6]:

$$F_{ij}^{\text{BAO}} = \sum_k \frac{\partial \ln(H(z_k))}{\partial p_i} \frac{\partial \ln(H(z_k))}{\partial p_j} \left( \frac{1}{\sigma_{\ln(H(z_i))}} \right)^2 + \frac{\partial \ln(d_A(z_k))}{\partial p_i} \frac{\partial \ln(d_A(z_k))}{\partial p_j} \left( \frac{1}{\sigma_{\ln(d_A(z_i))}} \right)^2 \quad (44)$$

Again the index  $k$  denotes the observables, which are binned into several redshift bins.  $p_i$  denotes the cosmological parameters.  $\sigma_{\ln(H(z))}$  and  $\sigma_{\ln(d_A(z))}$  are the errors (including the observational errors and the systematic errors) of the observables  $\ln(H(z))$  and  $\ln(d_A(z))$ , respectively. In order to study the detection ability of the BAO method, we shall consider the potential observations of a typical project, the final JDEM (Joint Dark Energy Mission) project [6], which is expected to survey 10000 deg<sup>2</sup> in the redshift range  $z \in (0.5, 2)$ . In the calculation, we bin the observables  $\ln(H(z))$  and  $\ln(d_A(z))$  into 10 redshift bins, i.e.  $\Delta z = 0.15$  for each bin. The calculation of the theoretical values of these quantities are straightforward. For the errors of these observable data, we use the fitting formulae derived in [28] (see also Eq. (4.8) in [6]).

The results of the Fisher information matrix are shown in Table VI. To begin with we consider a simple case with only two free parameters ( $w_0$ ,  $w_a$ ). We assume that the other parameters ( $\Omega_m$ ,  $\Omega_k$ ,  $h_0$ ) are fixed to their fiducial values. By using the Fisher matrix in Table VI, we obtain the

TABLE VI: BAO Fisher matrix

|            | $w_0$                  | $w_a$                  | $\Omega_m$             | $\Omega_k$             | $h_0$                  |
|------------|------------------------|------------------------|------------------------|------------------------|------------------------|
| $w_0$      | $0.193253 \times 10^4$ | $0.471352 \times 10^3$ | $0.865506 \times 10^4$ | $0.288000 \times 10^4$ | $0.125880 \times 10^5$ |
| $w_a$      | $0.471352 \times 10^3$ | $0.123299 \times 10^3$ | $0.234243 \times 10^4$ | $0.788613 \times 10^3$ | $0.309758 \times 10^4$ |
| $\Omega_m$ | $0.865506 \times 10^4$ | $0.234243 \times 10^4$ | $0.457760 \times 10^5$ | $0.153244 \times 10^5$ | $0.579934 \times 10^5$ |
| $\Omega_k$ | $0.288000 \times 10^4$ | $0.788613 \times 10^3$ | $0.153244 \times 10^5$ | $0.541597 \times 10^4$ | $0.190452 \times 10^5$ |
| $h_0$      | $0.125880 \times 10^5$ | $0.309758 \times 10^4$ | $0.579934 \times 10^5$ | $0.190452 \times 10^5$ | $0.834616 \times 10^5$ |

uncertainties of the free parameters:

$$\Delta w_0 = 0.087, \quad \Delta w_a = 0.346, \quad z_p = 0.323, \quad \Delta w_p = 0.023. \quad (45)$$

However, if we try to constrain all five parameters by BAO observations, the uncertainties of the parameters will become fairly large. For instance, the uncertainties of  $w_0$  and  $w_a$  become  $\Delta w_0 = 0.850$  and  $\Delta w_a = 3.611$ , respectively, which are much larger than those in (45). Similarly to the discussion in Sec. IID, we can consider the combination of the BAO observation and the Planck CMB prior. By analogous steps we obtain the results

$$\Delta w_0 = 0.176, \quad \Delta w_a = 0.415, \quad \Delta \Omega_m = 2.01 \times 10^{-2}, \quad \Delta \Omega_k = 6.40 \times 10^{-4}, \quad \Delta h_0 = 2.57 \times 10^{-2}. \quad (46)$$

The best pivot redshift and the value of  $\Delta w_p$  are

$$z_p = 0.664, \quad \Delta w_p = 0.059. \quad (47)$$

## B. Detection of dark energy by potential SNIa observations

Now, let us turn to discuss the detection of dark energy parameters by the SNIa probe. Type Ia supernovae serve as a standard candle of (approximately) known luminosity. The redshift of supernova can be obtained by studying its spectral lines. Thus the redshift-distance relation can be gotten from SNIa surveys. Now, SNIa observed from various experiments have been used successfully to deduce the acceleration of the universe after  $z = 1$  [1, 29]. In the near future, observations of SNIa are expected to be significantly improved, so that they will continue to serve as one of the most important methods for the determination of dark energy.

The observables for SNIa data are the apparent magnitudes  $m$ , which can be corrected to behave as standard candles with absolute magnitude  $M$  with  $m = M + \mu(z)$ . The function  $\mu(z)$  for the

measured redshift is

$$\mu(z) = 5 \log_{10}(d_L(z)) + 25, \quad (48)$$

where  $d_L$  is the luminosity distance. In this paper, we shall consider SNIa observations by the future SNAP (Supernova/Accelerating Probe) project [30]. As suggested by the SNAP group, we consider 300 low redshift supernovae, uniformly distributed over  $z \in (0.03, 0.08)$ . The error bar on the magnitude is assumed to be  $\sigma_m = 0.15$  mag. In addition, 2000 high redshift supernovae in the range  $z \in (0.1, 1.7)$  are considered. The expected redshift distribution of these sources can be found in the SNAP white book (the middle red curve in Fig. 9 of [30]). We bin these 2000 sources into 10 redshift bins in the range  $z \in (0.1, 1.7)$ . The total errors of the observables  $\sigma(z)$  can be estimated as follows [30, 31]:

$$\sigma = \sqrt{\sigma_1^2 + \sigma_2^2}, \quad (49)$$

where  $\sigma_1 = 0.15 \text{ mag}/\sqrt{N}$  ( $N$  is the total number of supernovae in each bin) is the intrinsic random Gaussian error, and  $\sigma_2 = 0.02 \text{ mag}(1+z)/2.7$  is the error due to the astrophysical systematics.

Thus, we can build a Fisher information matrix, which is

$$F_{ij}^{\text{SN}} = \sum_k \frac{\partial \mu(z_k)}{\partial p_i} \frac{\partial \mu(z_k)}{\partial p_j} \left( \frac{1}{\sigma(z_k)} \right)^2. \quad (50)$$

The results are shown in Table VII. The errors of the cosmological parameters are estimated by  $\Delta p_i = \sqrt{(F^{\text{SN}})^{-1}_{ii}}$ . Similar to Sec. III A, we first discuss the simplest case with two free parameters ( $w_0, w_a$ ). The results are

$$\Delta w_0 = 0.054, \quad \Delta w_a = 0.302, \quad z_p = 0.211, \quad \Delta w_p = 0.012. \quad (51)$$

To constrain all five cosmological parameters, we consider the combination of SNIa and the Planck CMB prior to decouple the degeneracy between  $(w_0, w_a)$  and the other parameters. The errors of the parameters are

$$\Delta w_0 = 0.051, \quad \Delta w_a = 0.201, \quad \Delta \Omega_m = 3.49 \times 10^{-3}, \quad \Delta \Omega_k = 6.52 \times 10^{-4}, \quad \Delta h_0 = 3.39 \times 10^{-3}. \quad (52)$$

We find that the values of  $\Delta w_0$  and  $\Delta w_a$  in (52) are close to those in (51). The best pivot redshift and the value of  $\Delta w_p$  are also obtained

$$z_p = 0.313, \quad \Delta w_p = 0.019. \quad (53)$$

TABLE VII: SNIa Fisher matrix

|            | $w_0$                  | $w_a$                  | $\Omega_m$             | $\Omega_k$             | $h_0$                  |
|------------|------------------------|------------------------|------------------------|------------------------|------------------------|
| $w_0$      | $0.703955 \times 10^4$ | $0.122773 \times 10^4$ | $0.207309 \times 10^5$ | $0.669019 \times 10^4$ | $0.522067 \times 10^5$ |
| $w_a$      | $0.122773 \times 10^4$ | $0.225085 \times 10^3$ | $0.377761 \times 10^4$ | $0.115185 \times 10^4$ | $0.849589 \times 10^4$ |
| $\Omega_m$ | $0.207309 \times 10^5$ | $0.377761 \times 10^4$ | $0.636028 \times 10^5$ | $0.194262 \times 10^5$ | $0.146902 \times 10^6$ |
| $\Omega_k$ | $0.669019 \times 10^4$ | $0.115185 \times 10^4$ | $0.194262 \times 10^5$ | $0.639862 \times 10^4$ | $0.498026 \times 10^5$ |
| $h_0$      | $0.522067 \times 10^5$ | $0.849589 \times 10^4$ | $0.146902 \times 10^6$ | $0.498026 \times 10^5$ | $0.491151 \times 10^6$ |

### C. Comparison with the ET GW observations

Now let us compare the detection abilities of various probes: GW, BAO and SNIa. First we consider the simplest case, where only dark energy parameters ( $w_0$ ,  $w_a$ ) are considered. The errors of the parameters are given in (45) for BAO, and in (51) for SNIa. We find that the values of  $\Delta w_0$ ,  $\Delta w_a$  and  $\Delta w_p$  are all smaller for the SNIa probe. This shows that, comparing with the JDEM BAO project, the SNAP SNIa project is expected to give a tighter constraint on the dark energy. For the ET GW project, in Sec. II C, we have considered four cases. For the optimistic case (strong beaming and uniform distribution of sources), the results are given in (33) and (34). As it turns out, the values of  $\Delta w_0$ ,  $\Delta w_a$  and  $\Delta w_p$  are all close to those for the SNAP SNIa project, but much smaller than those of the JDEM BAO project. However, we should remember that in this optimistic case, we have assumed an idealized condition for the determination of the sources' luminosity distance (very tight beaming of shGRBs). On the other hand, if the pessimistic case (realistic case and non-uniform distribution) is considered, the results are shown in (36) and (37). The values of  $\Delta w_0$ ,  $\Delta w_a$  and  $\Delta w_p$  become closer to those for the JDEM BAO project, and  $\sim 60\%$  larger than those for the SNAP SNIa project in (51). We conclude that, in this case, the detection ability of ET GW method is close to that of the JDEM BAO project, but weaker than that of the SNAP SNIa project. This is mainly because the number of the GW standard sirens ( $\sim 1000$  as we have assumed) is smaller than that of the SNIa standard candles ( $\sim 2000$  at high redshift). In order to clearly show this, let us consider another case for ET GW method, where we assume that 2000 sources will be observed. We then obtain  $\Delta w_0 = 0.052$ ,  $\Delta w_a = 0.314$  and  $\Delta w_p = 0.014$ , which comes close to the projected uncertainties of the SNAP SNIa project given by (51).

We can also compare the results of these three probes, when considering the full 5 cosmological parameters and adopting the Planck CMB prior. In Fig. 2 (middle panel), we plot the

2-dimensional uncertainty contours of the parameters  $(w_0, w_a)$ , where for the ET GW method we have considered the optimistic case (strong beaming and uniform distribution). Similarly, we find that the red curve (GW+CMB) is close to the green one (SNIa+CMB), but much tighter than the black one (BAO+CMB). By comparing the results in (42), (46) and (52), we could also expect that, considering the pessimistic case (realistic case and non-uniform distribution) for the ET GW project, the red curve (GW+CMB) is tighter than the black one (BAO+CMB), but looser than the green one (SNIa+CMB). In Fig. 2 (right panel), we plot the results of the 2-dimensional uncertainty contours for the four combinations (CMB+BAO+SNIa, CMB+GW+BAO, CMB+GW+SNIa, GW+SNIa+BAO). We find that the first three combinations have similar results. However, the constraint on the dark energy parameters is much looser for combination of GW+SNIa+BAO, where the Planck CMB probe is absent. This panel shows that the CMB prior indeed plays a crucial role in the detection of dark energy.

Let us now combine all the four probes to constrain the cosmological parameters, including the dark energy parameters. If we consider the strong beaming case and the uniform distribution for the GW sources, we obtain the constraints on the dark energy parameters

$$\Delta w_0 = 0.038, \Delta w_a = 0.156, z_p = 0.292, \Delta w_p = 0.015. \quad (54)$$

This is the best constraint what we could expect to obtain. However, if we consider the realistic case and the non-uniform distribution for the GW sources, the constraints loosen to

$$\Delta w_0 = 0.045, \Delta w_a = 0.173, z_p = 0.313, \Delta w_p = 0.017. \quad (55)$$

In Fig. 3 (lower-right panel), we plot the 2-dimensional uncertainty contours of the parameters  $(w_0, w_a)$  for all the four cases. We find that the four curves are very close to each other; the relative weight of the GW probe is not very high for the combined methods.

Finally, we would like to know how much the ET GW probe can contribute in constraining all the five cosmological parameters  $(w_0, w_a, \Omega_m, \Omega_k, h_0)$ . In order to do so, we first calculate the constraints on the parameters by the combination of CMB+BAO+SNIa. We obtain

$$\Delta w_0 = 0.048, \Delta w_a = 0.184, \Delta \Omega_m = 3.46 \times 10^{-3}, \Delta \Omega_k = 5.91 \times 10^{-4}, \Delta h_0 = 3.36 \times 10^{-3}. \quad (56)$$

If we then add the contribution of the ET GW probe (strong beaming case and uniform distribution), the results become

$$\Delta w_0 = 0.038, \Delta w_a = 0.156, \Delta \Omega_m = 3.02 \times 10^{-3}, \Delta \Omega_k = 5.70 \times 10^{-4}, \Delta h_0 = 2.53 \times 10^{-3}. \quad (57)$$

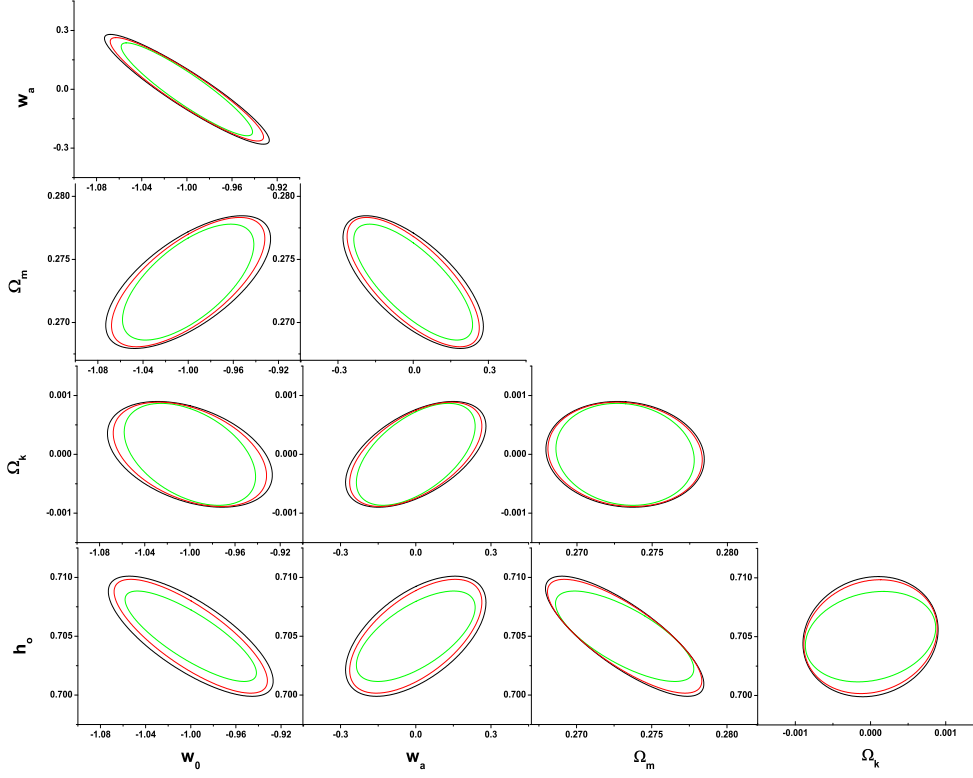


FIG. 4: The 2-d uncertainty contours of the cosmological parameters. The black (largest) curves denote the results of CMB+BAO+SNIa, and the red (middle) and green (smallest) curves denote the results of CMB+BAO+SNIa+GW. In the green (smallest) curve we have assumed the optimistic case (strong beaming case with uniform distribution), while in the red (middle) curve we have considered the pessimistic case (realistic case with non-uniform distribution).

We see a clear tightening of the constraints on all five parameters. In particular, the value of  $\Delta w_0$  is decreased by 20.8%, and that of  $\Delta w_a$  by 15.2%. On the other hand, if we assume the ET GW probe in the realistic case with the non-uniform distribution, the results are

$$\Delta w_0 = 0.045, \Delta w_a = 0.173, \Delta \Omega_m = 3.37 \times 10^{-3}, \Delta \Omega_k = 5.83 \times 10^{-4}, \Delta h_0 = 3.18 \times 10^{-3}. \quad (58)$$

In this case we find that, due to the contribution of ET GW probe,  $\Delta w_0$  is decreased by a 6.3% and  $\Delta w_a$  by 6.0%. In Fig. 4 we plot the 2-dimensional uncertainty contours of the free parameters ( $w_0, w_a, \Omega_m, \Omega_k, h_0$ ) for all three combinations.



#### IV. CONCLUSION

If short-hard  $\gamma$ -ray bursts (shGRBs) are produced by the mergers of neutron star binaries or binaries consisting of a neutron stars and a black hole, the luminosity distances  $d_L$  of the sources can be determined by the Einstein Telescope gravitational-wave detector in the redshift range  $z < 2$ . The redshifts  $z$  of the sources can be determined with great accuracy through their electromagnetic counterparts. Thus it will be possible to use shGRBs as ‘standard sirens’ to study the dark energy component in the universe by determining the EOS and its time evolution.

When calculating the uncertainties in the determination of  $d_L$  by the ET observations, we considered two case. One was the case of strong beaming, where the  $\gamma$  ray emission is assumed to be confined to a cone with a sufficiently small opening angle that for all practical purposes, the direction to the observer can be assumed perpendicular to the plane of the inspiral, i.e., the inclination angle  $\iota = 0$ . The other was the ‘realistic case’, which assumed that the opening angle of the beam could be as large as  $40^\circ$  [22], corresponding to inclination angles  $\iota < 20^\circ$ . In order to study the effect of the redshift distribution of the sources, we also considered two different kinds of distributions: one in which sources are distributed uniformly in comoving volume, and a non-uniform distribution as in [23]. We found that, by taking into account the Planck CMB prior, the errors on the dark energy parameters are expected to be  $\Delta w_0 = 0.053$  and  $\Delta w_a = 0.197$  in the optimistic case (strong beaming and uniform distribution of sources), which is close to the detection ability of the SNAP Type Ia Supernovae project. Even in the ‘pessimistic’ case (inclination angles up to  $20^\circ$  and non-uniform distribution of the sources), the errors are  $\Delta w_0 = 0.096$  and  $\Delta w_a = 0.296$ , which is weaker than the detection ability of the SNAP Type Ia Supernova project, but stronger than that of the JDEM Baryon Acoustic Oscillation project. We also found that, comparing with the combination of the future CMB(Planck)+BAO(JDEM)+SNIa(SNAP) projects, the contribution of this kind of standard sirens can decrease the error of  $w_0$  by  $\sim 6.3\%$  and that of  $w_a$  by  $\sim 6.0\%$ , even in the pessimistic case. Thus, the kind of self-calibrating GW standard sirens accessible to Einstein Telescope would provide an excellent probe of the dark energy component, and constitute an important complement to the general electromagnetic methods.

#### Acknowledgements

The authors thank L. P. Grishchuk and B. S. Sathyaprakash for stimulating discussions. WZ is partially supported by Chinese NSF Grants No. 10703005, No. 10775119, No. 11075141, and

the Foundation for University Young Teaching Excellence of the Ministry of Education, Zhejiang Province. CVDB and TGFL are supported by the research programme of the Foundation for Fundamental Research on Matter (FOM), which is partially supported by the Netherlands Organisation for Scientific Research (NWO).

- 
- [1] M. Kowalski et al., *Astrophys. J.* **686**, 749 (2008); M. Hicken et al., *Astrophys. J.* **700**, 1097 (2009).
  - [2] E. Komatsu et al. [WMAP Collaboration], arXiv:1001.4538.
  - [3] D. J. Eisenstein et al. [SDSS Collaboration], *Astrophys. J.* **633**, 560 (2005); W. J. Percival et al., *MNRAS* **381**, 1053 (2007).
  - [4] T. Schrabback et al., arXiv:0911.0053; M. Kilbinger et al., *A&A* **497**, 677 (2009).
  - [5] E. J. Copeland, M. Sami and S. Tsujikawa, *Int. J. Mod. Phys. D* **15**, 1753 (2006).
  - [6] A. Albrecht et al., *Report of the Dark Energy Task Force*, astro-ph/0609591.
  - [7] A. Refregier et al., *Euclid Imaging Consortium Science Book*, arXiv:1001.0061; P. A. Abell et al. [LSST Science Collaborations], *LSST Science Book, Version 2.0*, arXiv:0912.0201.
  - [8] B. Schutz, *Nature*, **323**, 310 (1986).
  - [9] S. Nissanke, S. A. Hughes, D. E. Holz, N. Dalal and J. L. Sievers, arXiv:0904.1017.
  - [10] C. L. MacLeod and C. J. Hogan, *Phys. Rev. D* **77**, 043512 (2008)
  - [11] D. E. Holz and S. A. Hughes, *Astrophys. J.* **629**, 15 (2005);
  - [12] N. Dalal, D. E. Holz, S. A. Hughes and B. Jain, *Phys. Rev. D* **74**, 063006 (2006)
  - [13] K. G. Arun, B. R. Iyer, B. S. Sathyaprakash, S. Sinha and C. Van Den Broeck, *Phys. Rev. D* **76**, 104016 (2007); K. G. Arun, C. K. Mishra, C. Van Den Broeck, B. R. Iyer, B. S. Sathyaprakash and S. Sinha, *Class. Quant. Grav.* **26**, 094021(2009);
  - [14] Chris Van Den Broeck, M. Trias, B. S. Sathyaprakash and A.M. Sintes, *Phys. Rev. D* **81**, 124031 (2010).
  - [15] C. Cutler and D. E. Holz, *Phys. Rev. D* **80**, 104009 (2009).
  - [16] *The Einstein Telescope Project*, <https://www.et-gw.eu/et/>.
  - [17] B. S. Sathyaprakash, B. F. Schutz and C. Van Den Broeck, arXiv:0906.4151.
  - [18] A. G. Riess et al., *Astron. J.* **116**, 1009 (1998); S. Perlmutter et al., *Astrophys. J.* **517**, 565 (1999).
  - [19] B. S. Sathyaprakash and B. F. Schutz, *Living Rev. Relativity* **12**, 2 (2009).
  - [20] A. Freise et al., arXiv:0908.0353.
  - [21] L. S. Finn, *Phys. Rev. D* **46**, 5236 (1992); L. S. Finn and D. F. Chernoff, *Phys. Rev. D* **47**, 2198 (1993).
  - [22] E. Nakar, *Phys. Rep.* **442**, 166 (2007).
  - [23] R. Schneider, V. Ferrari, S. Matarrese and S. F. Portegies Zwart, *MNRAS*, **324**, 797 (2001).
  - [24] Planck Collaboration, *The Scientific Programme of Planck*, astro-ph/0604069.

- [25] e.g. W. Zhao, D. Baskaran and L. P. Grishchuk, Phys. Rev. D **80**, 083005 (2009) (Appendix B).
- [26] M. Tegmark, A. Taylor and A. Heavens, Astrophys. J. **480**, 22 (1997); M. Zaldarriaga, D. Spergel and U. Seljak, Astrophys. J. **488**, 1 (1997).
- [27] M. Bartelmann and P. Schneider, Phys. Rep. **340**, 291 (2001); W. Hu and B. Jain, Phys. Rev. D **70**, 043009 (2004); D. Munshi, P. Valageas, L. Van Waerbeke and A. Heavens, Phys. Rep. **462**, 67 (2008).
- [28] C. Blake et al., MNRAS, **365**, 255 (2006).
- [29] M. Kowalski et al., Astrophys. J. **686**, 749 (2008); M. Hicken et al., Astrophys. J. **700**, 331 (2009).
- [30] SNAP Collaboration, *Supernova / Acceleration Probe: A Satellite Experiment to Study the Nature of the Dark Energy*, astro-ph/0405232.
- [31] E. V. Linder and D. Huterer, Phys. Rev. D **67**, 081303 (R) (2003).
- [32] More precisely, in the case of Einstein Telescope, binary neutron star signals can be in band for hours, but almost all of the signal-to-noise ratio will be accumulated in the final few minutes of the inspiral process.
- [33] This PSD corresponds to one possible design of ET; the same reference [20] also discusses alternatives.